

Cosmology and the Hubble Constant: On the Megamaser Cosmology Project (MCP)

C. Henkel¹, J.A. Braatz², M.J. Reid³, J.J. Condon⁴, K.Y. Lo⁵,
C.M.V. Impellizzeri⁶ and C.Y. Kuo⁷

¹Max-Planck-Institut für Radioastronomie, Auf dem Hügel 69, 53121 Bonn, Germany
Astron. Dept., King Abdulaziz University, P.O. Box 80203, Jeddah, Saudi Arabia
email: chenkel@mpifr-bonn.mpg.de

²National Radio Astronomy Observatory, 520 Edgemont Road,
Charlottesville, VA 22903, USA
email: jbraatz@nrao.edu

³Harvard-Smithsonian Center for Astrophysics, 60 Garden Street,
Cambridge, MA 02138, USA
email: reid@cfa.harvard.edu

⁴National Radio Astronomy Observatory, 520 Edgemont Road,
Charlottesville, VA 22903, USA
email: jcondon@nrao.edu

⁵National Radio Astronomy Observatory, 520 Edgemont Road,
Charlottesville, VA 22903, USA
email: flo@nrao.edu

⁶National Radio Astronomy Observatory, 520 Edgemont Road, Charlottesville,
VA 22903, USA
Joint ALMA Observatory, Alonso de Córdova 3107, Vitacura, Santiago, Chile
email: violette@nrao.edu

⁷Dept. of Astronomy, University of Virginia, Charlottesville, VA 22904, USA
AASIA, Astron.-Math. Building, Roosevelt Rd, Taipei 10617, Taiwan
email: ck2v@virginia.edu

Abstract. The Hubble constant H_0 describes not only the expansion of local space at redshift $z \sim 0$, but is also a fundamental parameter determining the evolution of the universe. Recent measurements of H_0 anchored on Cepheid observations have reached a precision of several percent. However, this problem is so important that confirmation from several methods is needed to better constrain H_0 and, with it, dark energy and the curvature of space. A particularly *direct* method involves the determination of distances to local galaxies far enough to be part of the Hubble flow through water vapor (H₂O) masers orbiting nuclear supermassive black holes. The goal of this article is to describe the relevance of H_0 with respect to fundamental cosmological questions and to summarize recent progress of the “Megamaser Cosmology Project” (MCP) related to the Hubble constant.

Keywords. masers, galaxies: active, galaxies: ISM, galaxies: nuclei, cosmology: cosmological parameters, cosmology: distance scale, radio lines: galaxies

1. Cosmological Background

For 85 years, it has been known that our universe is expanding (Lemaître 1927). This expansion was believed to slow down in time because of gravitational attraction. However, based on observations of luminous standard candles (Type Ia supernovae) Riess et al.

(1998) and Perlmutter et al. (1999) suggested instead accelerated expansion, turning cosmology upside down and winning the most recent Nobel Prize in physics. More than a decade after this discovery, accelerated expansion is well established. A de-acceleration during the initial few billion years after the “Big Bang”, when densities of matter and radiation were much higher than today, is followed by accelerated expansion. The cause of the accelerated expansion is so far unknown and is described by the term “Dark Energy”. Following the standard model, it should account for the majority of the energy density of the universe and retards the formation of large scale structure. Understanding dark energy may be the most important problem existing in physics today.

Dark Energy dominates the energy budget, accelerates the expansion of the universe, and affects large scale structure. What is its nature? There are three classes of potential explanations: (1) a cosmological constant, which has been proposed already in the early days of general relativity (Einstein 1917) as a kind of repulsive gravity, (2) a scalar field, somewhat analogous to that proposed to explain inflation at a much earlier time (e.g., Wetterich 1988; Ratra & Peebles 1988), and (3) modified gravity (e.g., Tsujikawa 2010), which will not be considered here.

Assuming that the universe is homogeneous and isotropic (as approximately suggested by the large scale matter distribution and the 3 K microwave background), the space-time metric can be written in the following form

$$ds^2 = dt^2 - a^2(t) \times [dr^2/(1 - kr^2) + r d\theta^2 + r^2 \sin^2\theta d\phi^2], \quad (1.1)$$

with t and $a \propto (1 + z)^{-1}$ being time and cosmic scale factor, r , θ , and ϕ denoting comoving spatial coordinates, and k representing the curvature of 3-dimensional space. The field equations of general relativity, applied to this Friedmann-Robertson-Walker metric, lead to the so-called Friedmann equations,

$$H = \left(\frac{\dot{a}}{a}\right)^2 = \frac{8\pi G}{3c^2} \rho - k \frac{c^2}{a^2} + \frac{\Lambda}{3} \quad (1.2)$$

and

$$\frac{\ddot{a}}{a} = -\frac{4\pi G}{3c^2} (\rho + 3p) + \frac{\Lambda}{3}. \quad (1.3)$$

H is the Hubble parameter for a given time (H_0 stands for redshift $z = 0$), ρ is the density of matter and radiation, p denotes pressure, and Λ represents the traditional cosmological constant, which (like dark energy) can be subsumed into the density and pressure term,

$$\frac{\ddot{a}}{a} = -\frac{4\pi G}{3c^2} \sum_i^n (\rho_i + 3p_i). \quad (1.4)$$

Defining $w = p/\rho$, the different (in part putative) components yield:

$$\begin{aligned} \text{Matter: } w &= 0 \\ \text{Radiation: } w &= 1/3 \\ \text{“Quintessential” scalar field: } w &< -1/3 \\ \text{Cosmological constant: } w &= -1 \\ \text{Phantom energy: } w &< -1 \end{aligned}$$

The resulting values of w determine the normalized acceleration \ddot{a}/a . For gravity (matter) we obtain the expected negative value. This also holds for radiation, which has dominated, according to the standard model, at redshifts $\gtrsim 10^4$. The $(\rho + 3p)$ term in Eq. 1.4 directly infers that w values smaller than $-1/3$ are required for accelerated expansion,

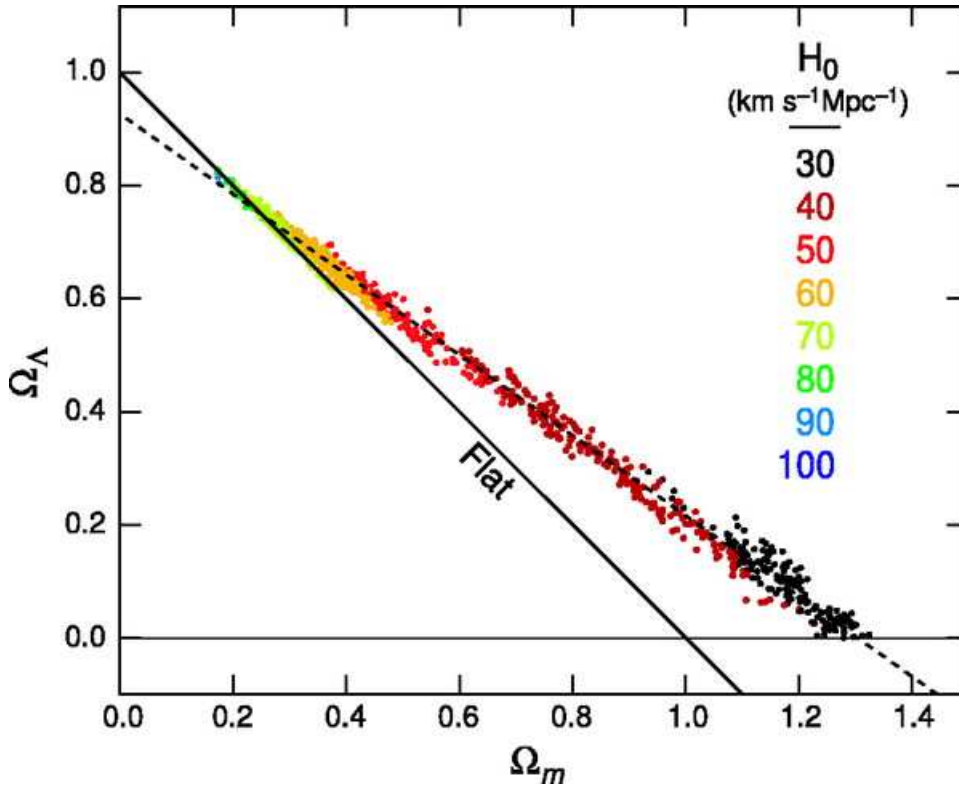


Figure 1. Constraints from the cosmic microwave background (Spergel et al. 2007). The different colors correspond to different values of the Hubble constant H_0 . Ω_m is the energy density of baryonic and dark matter in units of the critical density, Ω_Λ is the corresponding parameter for dark energy. For a “flat” universe, $\Omega_m + \Omega_\Lambda = 1$. The data are consistent with a wide range of H_0 values.

which is therefore the possible w range for dark energy. w and H , and thus also H_0 , are obviously related, emphasizing the cosmological importance of the Hubble constant.

Fig. 1 shows the range of not necessarily flat cosmological cold dark matter (CDM) models consistent with Wilkinson Microwave Anisotropy Probe (WMAP) data (Spergel et al. 2007). Assuming that the universe is flat would provide a rather accurate solution, but is it really flat as suggested by inflationary models? The present value of the curvature radius, R_0 , is related to H_0 and $\Omega_0 = \Omega_m + \Omega_\Lambda$ (see Fig. 1 for definitions) by

$$R_0 = (a/2) \times |k|^{-1/2} = (c/2) \times H_0^{-1} \times (\Omega_0 - 1)^{-1/2}. \quad (1.5)$$

c is the speed of light and $(c/2) \times H_0^{-1} \sim 2.1$ Gpc is known as the Hubble radius. Obviously, with our present precision to determine Ω_0 , curvature radii as small 10 Gpc cannot be excluded and we are still far from being able to state that the universe is truly flat. All this implies that the cosmic microwave background alone does not provide stringent limits. This is not unexpected, since the CMB provides information at a single early epoch, when dark energy did not play a role. Its importance can only be deduced by a combination of CMB observations with data from the much younger universe.

There are several lines of observational activity to constrain the wide range of models permitted by the CMB: These include (1) Type Ia supernovae, the standard candles, where luminosity distances and redshifts can be compared; (2) galaxy clusters, where

redshift independent ratios between baryonic and dark matter masses can only be obtained with a small subset of possible cosmologies; (3) gravitational lensing or cosmic shear, where the dark matter distribution can be determined, isolating dark energy; and (4) baryon acoustic oscillations (BAO), which left an imprint on the cosmic microwave background, which is clearly seen in CMB power spectra (e.g., Spergel et al. 2003, 2007; Komatsu et al. 2011). This imprint is still visible affecting structure at moderate redshifts and providing a local size scale of order 140 Mpc. All these tracers are observed at significant redshifts. However, it is at redshift zero where dark energy is most dominant, and only here its energy density is significantly higher than that of baryonic and dark matter combined. Thus it is the Hubble constant, providing a measure of the *local* universe, which provides the longest lever arm with respect to the CMB to measure the effects of dark energy (Hu 2005).

2. Constraining H_0

Assuming a Λ cold dark matter universe and excluding curvature, exotic neutrino or specific early universe physics, Komatsu et al. (2011) derive from WMAP data $H_0 = 71.0 \pm 2.5 \text{ km s}^{-1} \text{ Mpc}^{-1}$. While studies based on gravitational lens time delays (e.g., Treu & Koopmans 2002; Cardone et al. 2002) and on X-ray and Sunyaev-Zel'dovich data of galaxy clusters (e.g., Bonamente et al. 2006) have been used to constrain H_0 , such deductions from redshifted objects depend on the chosen cosmological model and are no substitute for a measurement of H_0 in the local universe.

With the HST key project to measure the Hubble constant, Freedman et al. (2001) obtained from Cepheids in nearby galaxies $H_0 = 72 \pm 3_r \pm 7_s \text{ km s}^{-1} \text{ Mpc}^{-1}$, estimating both random and systematic errors. This was based on the extragalactic distance ladder using Cepheid variable stars in the Large Magellanic Cloud to calibrate the measurements. However, the LMC has a low metallicity and significant depth. A potential dependence of Cepheid luminosities on metallicity and uncertainties in the distances to individual stars complicate the calibration. This was highlighted by Sandage et al. (2006), who used similar methods but a different metallicity correction to obtain $H_0 = 62 \pm 1.3_r \pm 5.0_s \text{ km s}^{-1} \text{ Mpc}^{-1}$ (Fig. 2). While the H_0 value by Freedman et al. (2001) is consistent with a flat universe, the Sandage et al. (2006) result challenges it.

To date the most ambitious program to determine H_0 is that led by A.G. Riess (see also Freedman & Madore 2010 for a recent review). Based on three anchors, (1) the parallax determinations of Galactic Cepheids, (2) Cepheids in the LMC with distances deduced from eclipsing binaries, (3) the distance to NGC 4258 (see Sect. 3) and with new *HST* (Hubble Space Telescope) data from galaxies with Cepheids *and* Type Ia supernovae, Riess et al. (2011) derive $H_0 = 73.8 \pm 2.4 \text{ km s}^{-1} \text{ Mpc}^{-1}$. This estimate also makes use of Cepheids measured in the near infrared, which helps to reduce both systematic and random errors with respect to optical observations. Note that the distance to NGC 4258 has been slightly revised in the meantime (E.M.L. Humphreys, priv. comm.).

While all these measurements are highly encouraging and pave the way to a more precise knowledge of our universe, a totally independent measure of H_0 is essential to either confirm the above cited results or to hint at problems that may have been overlooked so far.

3. The Megamaser Cosmology Project (MCP)

The MCP is an NRAO (National Radio Astronomy Observatory) key project to determine H_0 by measuring geometric distances with an accuracy of $\sim 10\%$ to ~ 10 galaxies

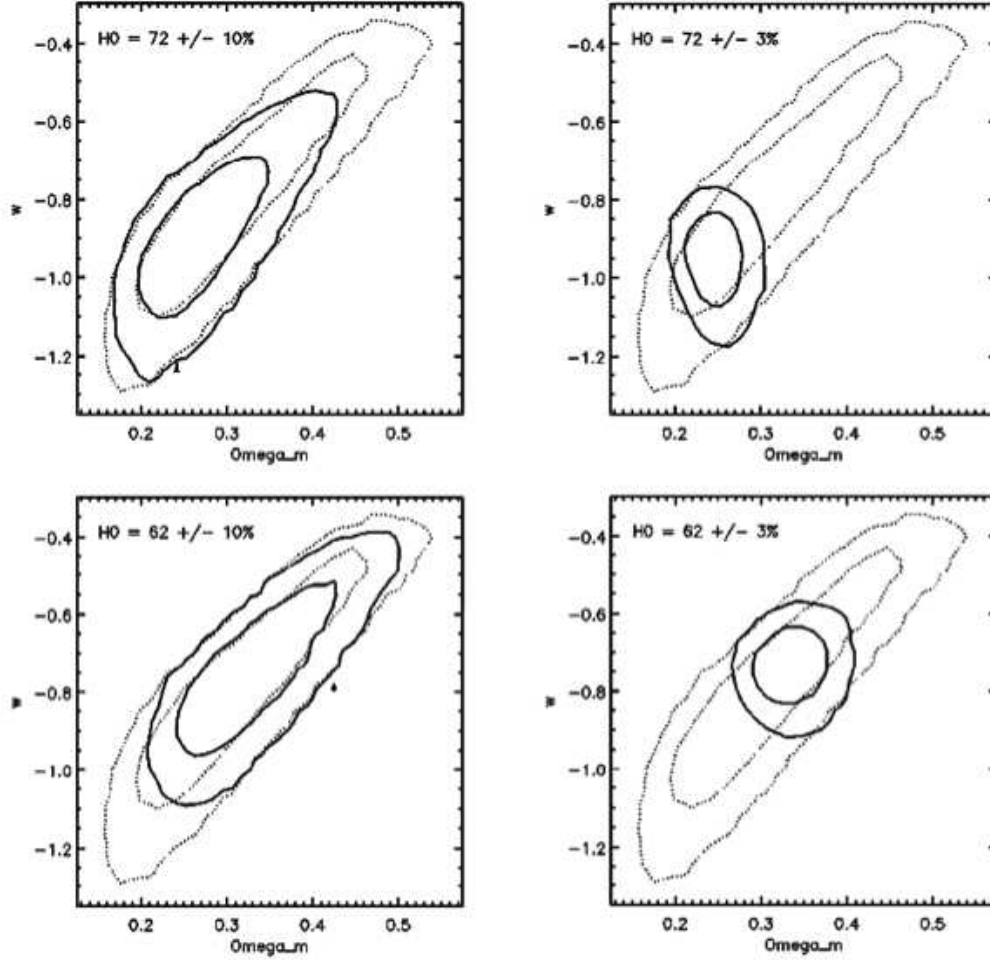


Figure 2. WMAP (Wilkinson Microwave Anisotropy Probe) 1σ and 2σ likelihood surfaces for Ω_m (see Fig. 1) and w (Eq. 1.4), with priors on H_0 (upper panels: $72 \text{ km s}^{-1} \text{ Mpc}^{-1}$; lower panels: $62 \text{ km s}^{-1} \text{ Mpc}$). Right versus left panels (solid lines) demonstrate the improvements gained by reducing the uncertainty in H_0 from 10% to 3%. Dotted lines: “wcdm + no perturbations” model from Spergel et al. (2007); solid lines: the same, but with constraints from H_0 incorporated.

in the local Hubble flow. Following the experience gained by studying the prototypical source, NGC 4258 (Miyoshi et al. 1995; Herrnstein et al. 1999), it includes (1) a GBT (Green Bank Telescope) survey to identify suitable circumnuclear 22 GHz H_2O maser disks (see Fig. 3 for a spectrum), (2) direct imaging of these sub-pc disks, using the VLBA (Very Long Baseline Array), the GBT, and, for northern sources, also the *Effelsberg* telescope, (3) GBT monitoring to measure accelerations of the spectral components, and (4) model calculations to simulate the maser disk dynamics. So far published articles include Reid et al. (2009), Braatz et al. (2010), Greene et al. (2010), and Kuo et al. (2011).

The 22 GHz H_2O “megamasers”, luminous masers associated with active galactic nu-

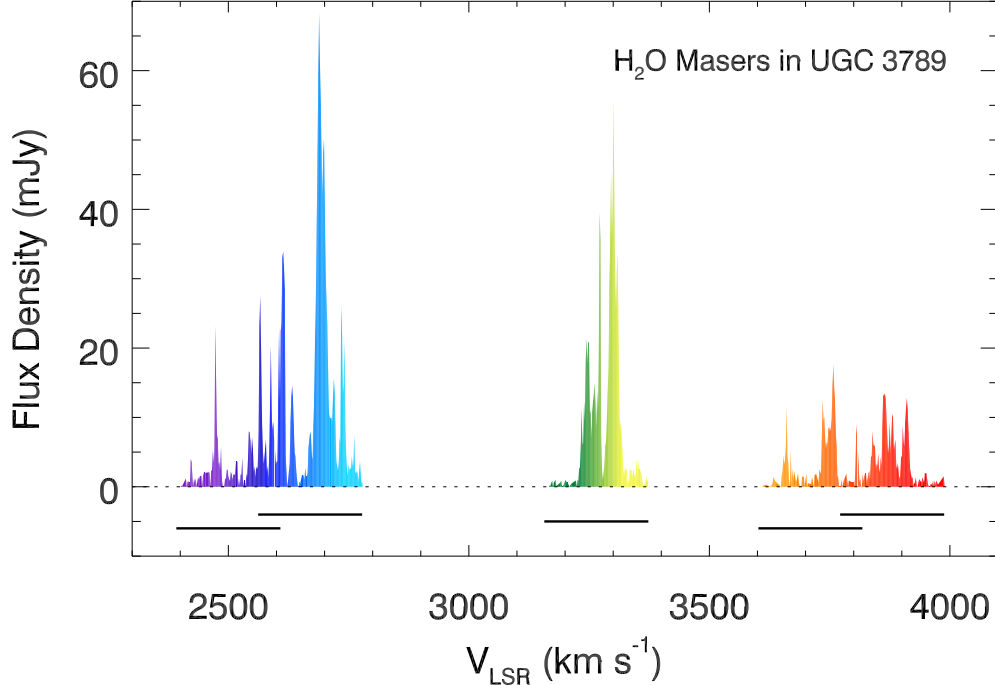


Figure 3. One of the newly found maser disks with systemic (green-yellow) and high velocity (violet-blue and orange-red) components.

clei, are mostly found in Seyfert 2 and LINER (Low Ionization Nuclear Emission Line Region) galaxies with high column densities (Braatz et al. 1997; Zhang et al. 2006; Madejski et al. 2006; Greenhill et al. 2008), relatively high optical luminosity, velocity dispersion, and $[\text{OIII}]\lambda 5007$ luminosity (Zhu et al. 2011) as well as relatively strong Fe $K\alpha$ lines in those sources which are Compton thick (Zhang et al. 2010). Low X-ray/ $[\text{OIV}]\lambda 25890$ ratios (Ramolla et al. 2011), and high nuclear radio continuum luminosities (Zhang et al. 2012) with respect to H_2O undetected galaxies are also statistically obtained.

The H_2O masers reside in thin, edge-on gaseous annuli. Emission near the systemic velocity of the parent galaxy originates from the near side of the disk and red- and blue-shifted satellite lines come from the two tangent points (see Figs. 3–5). Assuming an ideal circular, warpless thin disk, seen perfectly edge-on, and in Keplerian motion, the mass M_{AGN} enclosed by the disk is

$$M_{\text{AGN}} = 1.12 \times \left[\frac{V_{\text{rot}}}{\text{km s}^{-1}} \right]^2 \times \left[\frac{R}{\text{mas}} \right] \times \left[\frac{D}{\text{Mpc}} \right] M_{\odot}, \quad (3.1)$$

with V_{rot} denoting the rotation velocity at angular radius R and D representing the distance. Very long baseline interferometry maps allow us to directly measure V_{rot} for various values of R . From the Keplerian rotation curve we then obtain the constant

$$C_1 = \left[\frac{V_{\text{rot}}}{\text{km s}^{-1}} \right] \times \left[\frac{R}{\text{mas}} \right]^{1/2}. \quad (3.2)$$

The velocity gradient of the systemic features as a function of impact parameter provides

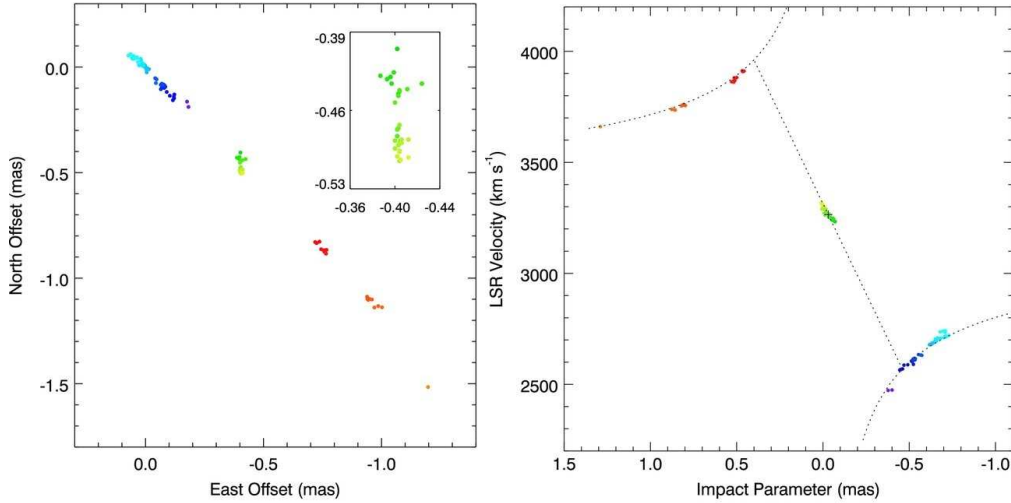


Figure 4. Left panel: H₂O image of the maser disk in UGC 3789 (from Reid et al. 2009). The insert presents a magnification of the systemic features. Right panel: Radial velocity versus impact parameter (also Reid et al. 2009). For the blue- and red-shifted high velocity components, Keplerian $r^{-1/2}$ rotation curves are also displayed.

another constant,

$$C_2 = \left[\frac{V_{\text{rot}}}{\text{km s}^{-1}} \right] \times \left[\frac{R}{\text{mas}} \right]^{-1}. \quad (3.3)$$

$C_1/C_2 = R^{3/2}$ then gives the angular radius R_s of the systemic features as viewed from a direction in the plane of the disk, but perpendicular to the line of sight. The total distance to the galaxy is then determined by the centripetal acceleration

$$dV_s/dt = \frac{V_{\text{rot}}^2}{r_s}, \quad (3.4)$$

with the index “s” denoting the systemic maser components. With dV_s/dt being measured, the linear scale r_s can be compared with the angular scale R_s to provide the preliminary distance estimate.

While such a procedure leads to a rough first estimate, disks may be warped (see Miyoshi et al. 1995 for the first such case, NGC 4258), orbits may be eccentric, and inclinations may not equal 90° . To model the circumnuclear disks as seen in H₂O as detailed as possible, a Bayesian fitting procedure has been developed (M.J. Reid), using a Markov Chain Monte Carlo approach. A Metropolis Hastings algorithm is applied to choose successive trial parameters covering the parameter space. Fig. 6 displays such a simulation for NGC 6264. These very preliminary simulations indicate low eccentricities ($e < 0.1$).

For UGC 3789, Fig. 5 indicates two groups of systemic maser components, one with a higher acceleration than the other. Unlike in NGC 4258, the systemic features do not arise from a single ring segment with specific galactocentric radius. The distance to the galaxy can be derived separately for the two rings. These yield $D_1 = 50.2 \pm 7.7$ Mpc and $D_2 = 48.1 \pm 17.4$ Mpc. The weighted mean is $D_{\text{UGC3789}} = 49.9 \pm 7.0$ Mpc (14%). With a peculiar radial velocity relative to the cosmic microwave background of -151

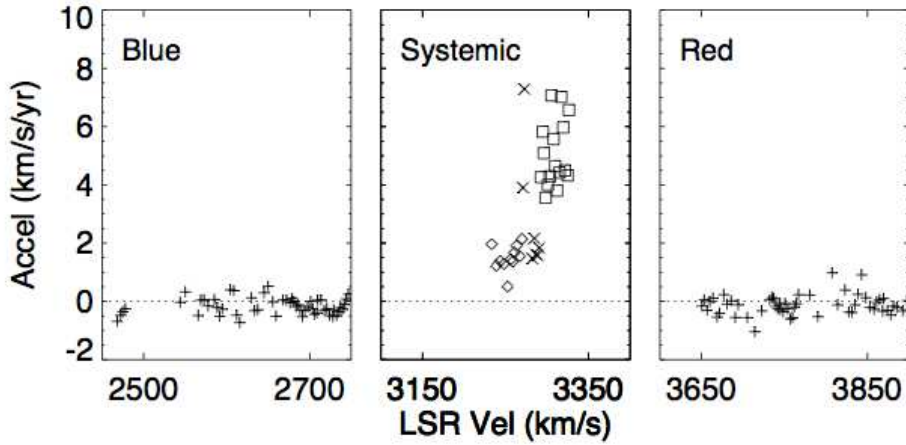


Figure 5. Acceleration of individual maser features in UGC 3789

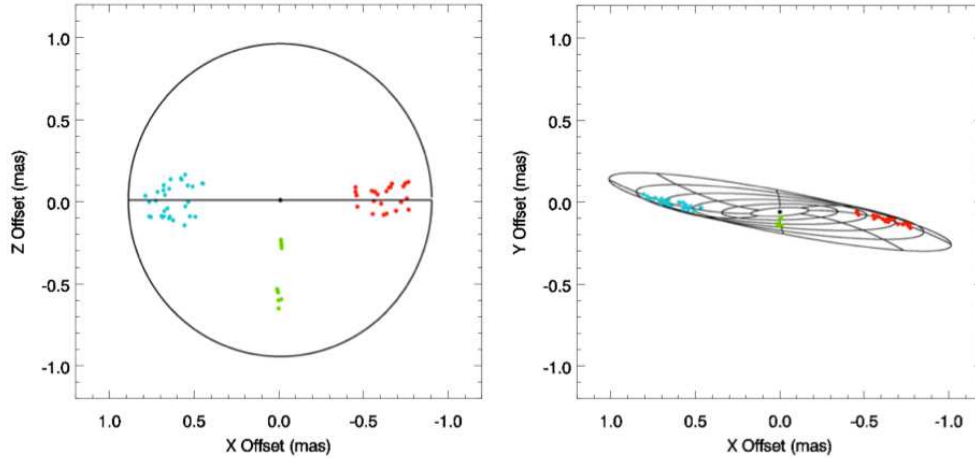


Figure 6. Bayesian fitting results of the maser disk in NGC 6264. Left panel: Face-on View onto the disk with systemic (green), approaching (blue) and receding (red) components. Right panel: Model of the warped disk viewed approximately edge-on as observed from Earth.

$\pm 163 \text{ km s}^{-1}$ and $V_{\text{CMB}} = V_{\text{LSR}} + 60 \text{ km s}^{-1}$, the relativistic, recessional flow velocity becomes $3481 \pm 163 \text{ km s}^{-1}$. This yields with standard Λ CDM parameters $H_0 = 69 \pm 11 \text{ Mpc}^{-1}$ (Braatz et al. 2010).

For NGC 6264, a source at a distance of 150 Mpc, a similar analysis results in $H_0 = 65.8 \pm 7.2 \text{ km s}^{-1}$ (Kuo 2011). Combining both sources, our present best estimate for the Hubble constant becomes $H_0 = 67 \pm 6 \text{ km s}^{-1}$. This preliminary result is so far consistent with all previously (Sect. 2) mentioned values.

4. Prospects

So far, two sources yielded publishable results. Increasing this number to 10 and accounting for the fact that the targets are located in different parts of the sky, the 1σ



Figure 7. The maser disk of NGC 4258 (Argon et al. 2007), extended east-west, and below the maser disk of NGC6323, extended approximately north-south, on the same angular scale. The given beam shows a typical synthesized beam for a high-declination target at 22 GHz using the *VLBA*, the *GBT*, and *Effelsberg*. The sketch emphasizes the great progress achieved in recent years when mapping H_2O maser emission in distant sources.

error of $6 \text{ km s}^{-1} \text{ Mpc}^{-1}$ obtained so far should decrease by a factor of $(2/10)^{1/2}$ to $\sim 2.7 \text{ km s}^{-1} \text{ Mpc}^{-1}$ or 4%. Longer monitoring and more interferometric maps can reduce this uncertainty further. To demonstrate the degree of sensitivity required for these measurements, Fig. 7 shows the size of the prototypical nuclear disk in NGC 4258 on the same angular scale as the disk toward NGC 6323. While NGC 4258 is with $V \sim 500 \text{ km s}^{-1}$ not yet in the Hubble flow and therefore not useful for a direct H_0 estimate (its maser lines are nevertheless essential to calibrate the distance scale defined by Cepheids), NGC 6323 has the potential to probe the distance scale with its recessional velocity of almost 7800 km s^{-1} . Toward NGC 6323, NGC 1194, NGC 2273, and Mrk 1419 the maser disks have also been mapped, demonstrating that the technique to derive distances, first tried out on NGC 4258, can also be used for much more distant galaxies.

Figs. 3, 5, and 7 directly demonstrate the importance of sensitivity. While in UGC 3789 many features have flux densities of $\sim 5 \text{ mJy}$ or higher, which can be readily analyzed, more distant sources reveal a plethora of components below this critical level. Getting these components as well would greatly facilitate any analysis. Thus the inclusion of a phased *Jansky VLA* (Very Large Array) is highly desirable. The completion of the Sardinia telescope may also help in the foreseeable future. Furthermore, as Fig. 7 indicates, angular resolution is another essential point. While an SKA-high would guarantee extreme sensitivity, the small angular extent of the H_2O maser disks requires a world-wide array, with space-VLBI providing another significant improvement.

Aside of the maser sources mentioned above, new targets have been detected, which look promising when analyzing their single dish spectra. While it remains to be seen how useful they will be for detailed mapping, it is worth mentioning that so far no systemic feature has been detected that shows a secular drift to the blue side. Either the nuclei are opaque at 22 GHz or the radiation is so highly beamed that maser photons from the backside of the disks have no chance to reach us.

References

Argon, A.L., Greenhill, L.J., Reid, M.J., et al. 2007, *ApJ*, 659, 1040

- Bonamente, M., Joy, M.K., LaRoque, S.J., et al. 2006, *ApJ*, 647, 25
- Braatz, J.A., Wilson, A.S., Henkel, C. 1996, *ApJS*, 110, 321
- Braatz, J.A., Reid, M.J., Humphreys, E.M.L. et al. 2010, *ApJ*, 718, 657
- Cardone, V.F., Capozziello, S., Re, V., & Piedipalumbo, E. 2002, *A&A*, 382, 792
- Einstein, A. 1917, *Sitzungsber. Königl. Preuß. Akad. der Wiss.*, 6, 142
- Freedman, W.L., & Madore, B.F. 2010, *ARA&A*, 48, 673
- Freedman, W.L., Madore, B.F., Gibson, B.K., et al. 2001, *ApJ*, 553, 47
- Greenhill, L.J., Tilak, A., & Madejski, G. 2008, *ApJ*, 686, L13
- Greene, J.E., Peng, C.Y., Kim, M. et al. 2010, *ApJ*, 721, 26
- Herrnstein, J.R., Moran, J.M., Greenhill, L.J. et al. 1999, *Nature*, 400, 539
- Hu, W. 2005, *ASP Conf. Ser.* 339, Observing Dark Energy, eds. S.C. Wolff & T.R.Lauer (San Francisco, ASP), 215
- Komatsu, E., Smith, K.M., Dunkley, J., et al. 2011, *ApJS*, 192, 1
- Kuo, C.Y. 2011, *Ph.D. Thesis*, Univ. of Virginia, Charlottesville
- Kuo, C.Y., Braatz, J.A., Condon, J.J. et al. 2011, *ApJ*, 727, 20
- Lemaître, G. 1927, *Annales de la Société Scientifique de Bruxelles*, 47, 49
- Madejski, G., Done, C., & Zycki, P.T. 2006, *ApJ*, 636, 75
- Miyoshi, M., Moran, J., Herrnstein, J. et al. 1995, *Nature*, 373, 127
- Perlmutter, S., Aldering, G., Goldhaber, G., et al. 1999, *ApJ*, 517, 565
- Ramolla, M., Haas, M., Bennert, V.N., & Chini, R., 2011 *A&A*, 530, 147
- Ratra, B. & Peebles, P.J.E. 1988 *Phys. Rev. D*, 37, 3406
- Reid, M.J., Braatz, J.A., Condon, J.J. et al. 2009, *ApJ*, 695, 287
- Riess, A.G., Filippenko, A.V., Challis, P., et al. 1998, *AJ*, 116, 1009
- Riess, A.G., Macri, L., Casertano, S., et al. 2011, *ApJ*, 730, 119
- Sandage, A., Tammann, G.A., Saha, A., et al. 2006, *ApJ*, 653, 843
- Spergel, D.N., Verde, L., Peiris, H.V., et al. 2003, *ApJS*, 148, 175
- Spergel, D.N., Bean, R., Doré, O., et al. 2007, *ApJS*, 170, 377
- Treu, T., & Koopmans, L.V.E. 2002, *MNRAS*, 337, L6
- Tsujikawa, S. 2010, *Lect. Notes in Phys.*, 800, 99
- Wetterich, C. 1988 *Nucl. Phys. B*, 302, 668
- Zhang, J.S., Henkel, C., Kadler, M., et al. 2006 *A&A*, 450, 933
- Zhang, J.S., Henkel, C., Gui, Q., et al. 2010 *ApJ*, 708, 1582
- Zhang, J.S., Henkel, C., Gui, Q., & Wang, J. 2012 *A&A*, 538, 152
- Zhu, G., Zaw, I., Blanton, M.R., & Greenhill, L.J. 2011 *ApJ*, 742, 73